ELSEVIER

Simulation of tropical Pacific and Atlantic Oceans using a HYbrid Coordinate Ocean Model

C. Shaji [a], C. Wang [b,*], G.R. Halliwell Jr. [c], A. Wallcraft [d]

[a] *Cooperative Institute for Marine and Atmospheric Studies, University of Miami, Miami, FL, USA*
[b] *Physical Oceanography Division, NOAA Atlantic Oceanographic and Meteorological Laboratory, 4301 Rickenbacker Causeway, Miami, FL 33149, USA*
[c] *Rosenstiel School of Marine and Atmospheric Science, University of Miami, Miami, FL, USA*
[d] *Naval Research Laboratory, Stennis Space Center, Mississippi, USA*

Abstract

The climatological annual cycle of the tropical Pacific and Atlantic Oceans is simulated using the HYbrid Coordinate Ocean Model (HYCOM) configured in a non-uniform horizontal grid spanning 30°S–65.5°N and 102°E–15°E. The model is initialized with climatological summer temperature and salinity and is forced by climatological atmospheric fields derived from the COADS and ECMWF ERA-15 reanalysis. The model is spun up for 20 years to reach a reasonable steady state in the primary region of interest from 20°S to 20°N, and year 20 is analyzed. The COADS simulation is primarily analyzed because it is slightly better in more respects than the ECMWF simulation, particularly in the representation of upper-ocean thermal structure. The model generally reproduces the seasonal variability of major circulation features in both oceans reasonably well when compared to climatologies derived from several observational datasets (surface drifters, TAO mooring array, COADS, Levitus, Pathfinder SST), and when compared to other model simulations. Model evaluation is complicated by the fact that the different climatologies, including the atmospheric reanalysis climatologies that drive the model, are averaged over different time intervals. In the tropics, the model thermocline reproduces the observed zonal slopes and meridional ridges/troughs in the thermocline. The simulated Equatorial Undercurrent compares favorably to observations, but is slightly deeper than observed. The model overestimates temperature in the Pacific warm pool regions, both

---

* Corresponding author. Tel.: +1 305 361 4325; fax: +1 305 361 4412.
E-mail address: chunzai.wang@noaa.gov (C. Wang).

1. REPORT DATE **MAY 2004**	2. REPORT TYPE	3. DATES COVERED **00-00-2004 to 00-00-2004**

4. TITLE AND SUBTITLE	5a. CONTRACT NUMBER
Simulation of tropical Pacific and Atlantic Oceans using a HYbrid Coordinate Ocean Model	5b. GRANT NUMBER
	5c. PROGRAM ELEMENT NUMBER
6. AUTHOR(S)	5d. PROJECT NUMBER
	5e. TASK NUMBER
	5f. WORK UNIT NUMBER

7. PERFORMING ORGANIZATION NAME(S) AND ADDRESS(ES) **Naval Research Laboratory,Oceanography Division,1002 Balch Boulevard,Stennis Space Center,MS,39522-5001**	8. PERFORMING ORGANIZATION REPORT NUMBER

9. SPONSORING/MONITORING AGENCY NAME(S) AND ADDRESS(ES)	10. SPONSOR/MONITOR'S ACRONYM(S)
	11. SPONSOR/MONITOR'S REPORT NUMBER(S)

12. DISTRIBUTION/AVAILABILITY STATEMENT
Approved for public release; distribution unlimited

13. SUPPLEMENTARY NOTES

14. ABSTRACT
see report

15. SUBJECT TERMS

16. SECURITY CLASSIFICATION OF:			17. LIMITATION OF ABSTRACT	18. NUMBER OF PAGES	19a. NAME OF RESPONSIBLE PERSON
a. REPORT **unclassified**	b. ABSTRACT **unclassified**	c. THIS PAGE **unclassified**	**Same as Report (SAR)**	**30**	

Standard Form 298 (Rev. 8-98)
Prescribed by ANSI Std Z39-18

west and east, by more than 1°C when compared to all observed climatologies. The model also tends to overestimate temperature in the eastern equatorial cold tongues in both the Atlantic and Pacific, with this overestimate being confined to a very small region of the far eastern Pacific during winter. This overestimate varies substantially depending on which observed climatology is used for the comparison, so model limitations are only partly responsible for the simulated–observed temperature differences in the cold tongues.

1. Introduction

Many studies have been performed using ocean models of various types to study the tropical Pacific and Atlantic Ocean circulation. Busalacchi and O'Brien (1980) used a linear, reduced gravity model without thermodynamics to simulate the equatorial current system in the tropical Pacific. The study revealed that linear dynamics is sufficient to understand many aspects of the influence of equatorially trapped Rosssby and Kelvin waves on the equatorial current system. Their relatively simple model was therefore capable of reproducing the location and variability of equatorial surface currents, but not important thermodynamical processes. Philander et al. (1987) forced a level coordinate primitive equation ocean general circulation model (OGCM) with seasonally varying climatological fields to study the mass and heat budget of the tropical Pacific. Broad features of the seasonal variability of the equatorial surface circulation and the thermocline movements were realistically obtained from their model study. Philander and Pacanowski (1986) used this same model to study the upper-ocean seasonal cycle of the tropical Atlantic.

Vertical mixing is very important for accurately simulating the baroclinic structure and flow field of the tropical ocean using OGCMs. Chen et al. (1994) studied the tropical circulation in the Pacific Ocean by embedding three different vertical mixing schemes in a 3-D ocean model. The mixing algorithms considered in their study are the Mellor–Yamada (MY) level 2.5 turbulence closure model (Mellor and Yamada, 1982), the Kraus–Turner (KT) bulk model (Turner and Kraus, 1967; Niiler and Kraus, 1977), and a hybrid method where Richardson number instability mixing from the dynamical instability model of Price et al. (1986) was included with the KT model to provide mixing beneath the bulk mixed layer. The hybrid scheme generated more realistic circulation features in the equatorial Pacific Ocean than the other mixing models. Murtugudde et al. (1995) applied a reduced gravity, isopycnal vertical coordinate ocean model to the three tropical oceans, neglecting salinity effects on density and representing the surface mixed layer by a constant depth layer. Individual simulations forced with climatic winds and surface heat fluxes based on observed sea surface temperature (SST) were conducted separately in the tropical Atlantic, Pacific, and Indian Oceans. The model reproduced most of the wind-driven currents and many features of the thermocline such as the annual cycle of zonal and meridional thermocline slope. However, the surface heat flux and vertical mixing parameterizations used in their model produced unrealistic SSTs, especially in the western boundary current regions.

It is important to further improve OGCMs to accurately simulate important climate processes occurring in the tropical ocean such as shallow meridional overturning cells. These cells are responsible for supplying water to the Equatorial Undercurrent (EUC) in both the Atlantic and Pacific Oceans. For example, Lu et al. (1998) investigated Pacific shallow overturning cells in a layer model study, documenting the importance of tropical and subtropical overturning cells in both the North and South Pacific for contributing water to the EUC. The present study revisits these and other issues by simulating the climatological annual cycles of the tropical Atlantic and Pacific Oceans using a new ocean general circulation model, specifically the HYbrid Coordinate Ocean Model (HYCOM; Bleck, 2002; Chassignet et al., 2003; Halliwell, 2004). This model contains a hybrid level-isopycnic-sigma vertical coordinate and contains several state-of-the-art vertical-mixing submodels. HYCOM has evolved from the Miami Isopycnic Coordinate Ocean Model (MICOM). Chassignet et al. (1996) compared MICOM to the GFDL level-coordinate model (Cox, 1984) in the Atlantic Ocean to demonstrate the advantages of isopycnic vertical coordinates in long climate integrations, particularly in regards to the inability of level coordinate models to retain their most dense water masses and produce a realistic meridional overturning circulation. Also, the MICOM simulation generated a stronger EUC that compared more favorably to observations than the GFDL model. HYCOM was created to correct known shortcomings of MICOM vertical coordinate system, which consists of isopycnic layers capped by a single slab mixed layer. In particular, isopycnic coordinates provide little or no vertical resolution in regions with weak stratification, including the surface mixed layer. HYCOM is designed to retain the advantages of isopycnic coordinates as much as possible in the open stratified ocean, but to transform into level (pressure) coordinates in unstratified regions such as the surface mixed layer, and also transform to terrain-following (sigma) coordinates in the coastal ocean.

Further details of the HYCOM equations and numerical algorithms, along with a description and validation of the hybrid coordinate generator, can be found in Bleck (2002). The several vertical mixing choices embedded in HYCOM are described and initially evaluated by Halliwell (2004). He demonstrates that the K-Profile Parameterization (KPP; Large et al., 1994), NASA GISS level 2 turbulence closure, MY level 2.5 turbulence closure, and Price et al. (1986) dynamical instability model all perform reasonably well in low resolution climatic simulations. Chassignet et al. (2003) demonstrate the flexibility of the hybrid grid generator by comparing HYCOM run in its default hybrid mode to HYCOM run as a level-coordinate and isopycnic-coordinate model. They also demonstrate the advantages of referencing HYCOM potential density to mid-depth pressure (20 MPa) and using the thermobaric compressibility correction of Sun et al. (1999) to calculate the pressure gradient force.

MICOM/HYCOM studies to date have focused primarily on middle and high latitude processes. In this study, we use HYCOM configured on a non-uniform grid to document the annual cycle of upper-ocean stratification and circulation in the tropical Pacific and Atlantic Oceans. The main goal is to evaluate HYCOM tropical ocean simulations when configured on a non-uniform grid designed to provide maximum meridional resolution near the equator. Since model errors and biases will be caused in part by errors and biases in the climatological forcing, this sensitivity is also examined by driving it with both the COADS climatology (Woodruff et al., 1987) and the ECMWF ERA-15 reanalysis climatology (Gibson et al., 1999). This initial study is designed to provide baseline results for planned HYCOM studies designed to evaluate sensitivity to vertical mixing choice, vertical coordinate distribution, and other HYCOM subgrid-scale

parameterizations. For example, HYCOM has recently been equipped with three new horizontal advection algorithms in addition to the MPDATA (Multidimensional Positive Definite Advection Transport Algorithm) used previously in MICOM and HYCOM. In Section 2, we describe the model configuration, the experiments, and the observations used to validate model results. The simulated tropical ocean circulation in the Pacific and Atlantic basins using COADS (Woodruff et al., 1987) forcing are evaluated in Sections 3 and 4 respectively. In Section 5, the COADS and ECMWF ERA-15 reanalysis simulations are compared to demonstrate that the COADS results are generally more realistic. Conclusions are presented in Section 6.

2. Model and observations

The HYCOM configuration for the numerical experiments, along with the observations used for comparison and validation, are described first.

2.1. Model configuration and numerical experiments

The computational domain spans the Pacific and Atlantic basins from 30°S to 65.5°N and 102°E to 15°E. The standard Mercator grid configuration used in earlier MICOM/HYCOM studies has been modified. The zonal grid resolution remains a uniform 0.72°, but the meridional grid resolution is set to 0.36° between 5°S and 5°N to improve the resolution of zonal equatorial currents. Poleward of 10°S and 10°N, the standard square Mercator grid is used where meridional resolution is $0.72 \cos \varphi$, where φ is latitude. Meridional resolution therefore gradually decreases from 0.36° to 0.72° in the bands from 5°S to 10°S and from 5°N to 10°N. The model is configured with 22 layers. Since we are interested exclusively in upper-ocean processes, we use a surface reference pressure for our target potential density (σ_0) values of 19.50, 20.25, 21.00, 21.75, 22.50, 23.25, 24.0, 24.70, 25.28, 25.77, 26.18, 26.52, 26.80, 27.03, 27.22, 27.38, 27.52, 27.64, 27.74, 27.82, 27.88, and 27.94. The target densities of the top five layers are chosen to be lighter than water encountered almost everywhere in the ocean so that they exist as level coordinates at the surface and provide reasonable vertical resolution in the surface mixed layer. The bottom topography is based on ETOPO5 data. The KPP vertical mixing model (Large et al., 1994) is used. Details regarding the implementation of KPP in HYCOM can be found in Halliwell (2004).

The model is initialized with summer temperature and salinity from the Levitus monthly climatology (Levitus and Boyer, 1994; Levitus et al., 1994) and run for 20 years. It is driven by monthly wind stress, wind speed, surface air temperature, surface atmospheric specific humidity, net shortwave radiation, net longwave radiation and precipitation fields obtained from both the COADS climatological dataset and ECMWF ERA-15 atmospheric reanalysis climatology. The sensible and latent heat fluxes are calculated during model runs using the model sea surface temperature (SST) and the same bulk aerodynamic formulae used in MICOM (Langlois et al., 1997). The northern and southern edges of the model domain are treated as closed boundaries. Boundary conditions are provided by buffer zones that are ten grid points wide within which temperature, salinity, and interface depth are relaxed to Levitus climatological values that have been vertically remapped to hybrid vertical coordinates. The relaxation time scale increases from 20 to 120 days with distance away from the boundaries.

Fields from the final year of the simulations (year 20) are analyzed here. For the purpose of conducting model–data comparisons, the simulated fields stored on the hybrid vertical coordinates are re-mapped onto level coordinates using vertical linear interpolation. In the following discussions in this article, wherever we mention seasons (winter, spring, summer and fall), we mean the boreal ones unless and otherwise specified.

2.2. Observations

We use several observational data sets to evaluate the model simulations. First, satellite-tracked surface drifters drogued at a depth of 15 m (Niiler, 2001) are compared to the simulated upper-ocean currents and temperature at 15 m. Climatological mean fields of surface currents and temperature are calculated from the drifters. The drifter observations of surface current are decomposed into a time-mean field, seasonal harmonics (annual and semi-annual) and a residual eddy field characterized by a finite integral time scale (Lumpkin, 2003). Climatological values for a given day are constructed from the time-mean field and the seasonal harmonics. From these, the monthly mean maps of currents and temperature are constructed. Further details regarding this calculation can be found in Lumpkin (2003).

In the Pacific Ocean, Acoustic Doppler Current Profiler (ADCP) horizontal velocity data are available from the Tropical Atmosphere Ocean (TAO) array (McPhaden et al., 1998). To evaluate the simulations, we use zonal velocity data from four of these arrays located in the eastern equatorial Pacific (110°W, 0°), east-central equatorial Pacific (140°W, 0°), west-central equatorial Pacific (170°W, 0°) and western equatorial Pacific (165°E, 0°). At these points monthly climatological velocities are prepared using daily data from 1991 to 2000. ADCP current data are presently unavailable in the equatorial Atlantic Ocean.

Also in the Pacific Ocean, daily subsurface temperature data are available along the equator from TAO moorings at 147°E, 156°E, 165°E, 180°W, 170°W, 155°W, 140°W, 125°W, 110°W and 95°W. We prepared the climatological monthly mean temperature at each location using daily data from 1991 to 2000 that were interpolated to fixed standard depths of 1, 10, 25, 50, 75, 100, 125, 150, 175, 200, 250, 300 and 500 m, and then gridded to 1° resolution from 147°E to 95°W. In the tropical Atlantic, we compare the Levitus (Levitus and Boyer, 1994) subsurface temperature data to the simulated temperature.

Sea surface temperature (SST) from the model is compared to SST from the Pathfinder (Casey and Cornillon, 1999) dataset. The NASA-funded SST Pathfinder project (Evans and Podesta, 1996) is designed to generate an accurate and consistent global SST dataset from measurements made by the AVHRR infrared instrument flown on NOAA satellites since November 1981. In situ SST measurements are used to optimize coefficients in the equation used to calculate Pathfinder SST from irradiance measurements in multiple infrared channels. SST fields are produced by first computing 4-km resolution Global Area Coverage (GAC) AVHRR SST retrievals, then binning cloud free retrievals into 9 km equal area fields twice daily (day and night). The global fields show zero bias and 0.5 °C rms with respect to cotemporal 1 m temperature measured by buoys. The climatology was created by averaging into monthly means, then calculating climatological monthly means over the 1985–1997 time interval. Both daytime and nighttime daily fields are included in each monthly average. A 7×7 point median filter is applied to fill in many of the gaps, and a 7×7 point median smoother is used for the entire field to remove small-scale noise.

3. Circulation in the tropical Pacific Ocean

The simulated circulation in the tropical Pacific Ocean is compared to observations, focusing first on the surface flow pattern and then on the subsurface structure.

3.1. Surface circulation

The surface circulation in the tropical Pacific Ocean is driven primarily by the trade wind pattern and consists of alternating bands of eastward and westward flowing zonal currents. These include the westward South Equatorial Current (SEC) and North Equatorial Current (NEC), which are the largest and most persistent zonal currents. The eastward flowing North Equatorial Countercurrent (NECC) and South Equatorial Countercurrent (SECC) often interrupt these broad westward flows. The strength and latitude bands of these currents depend strongly on the seasonal variability in the wind stress forcing. Fig. 1a and c display the simulated currents and temperature at 15 m during February and August while Fig. 1b and d display the corresponding fields derived from satellite-tracked drifters. From Fig. 1a and b similar major current features are present in both the model and observations during February. Simulated surface currents tend to be stronger than observed near the equator, but weaker away from the equator where meridional resolution is lower. The simulated SEC generally extends northward to about 5°N except in the far western Pacific where southeastward boundary flow exists south of the equator in both the simulation and observations and extends eastward into the interior from 8 to 12°S to about the middle of the basin as the SECC. In the eastern Pacific south of 10°S the model SEC is weaker than observed. Near the equator, both the model and observed SEC accelerates from the eastern Pacific to around 170°W with the surface divergence associated with equatorial upwelling clearly evident. The maximum SEC velocity reaches about 60 cm s^{-1} in the model and 70 cm s^{-1} in the observations although simulated currents tend to be stronger than observed over most of the tropical Pacific within a few degrees of the equator. The westward flowing NEC is evident north of 10°N in both the simulation and observations, and tends to weaken northward towards 20°N. Between 5°N and 10°N, the narrow eastward NECC extends across nearly the full width of the ocean. The simulated NEC and NECC are both weaker than observed.

The equatorial current system shows more seasonal variation in the western half of the basin. The simulated and observed NEC is weaker in August than in February because the Northern Hemisphere trade winds are weaker then. The simulated and observed SEC spans the full width of the ocean south of 5°S during August (Fig. 1c and d), with no SECC evident. In the western Pacific, the simulated and observed flow is eastward between 3°N and equator. The SEC in the central and eastern part of the basin is more intense during August because the southeasterly trades are stronger in boreal summer. The simulated and observed SEC attains a maximum velocity of about 1 m s^{-1} along the equator in August, but simulated flow tends to be stronger than observed near the equator west of about 130°W. As during February, the August SEC accelerates in the eastern Pacific to about 160°W with equatorial divergence clearly evident. The SEC turns north of the equator around 150°W, and then eastward to supply water to the NECC and thus close the western end of an anticyclonic (equatorial) gyre. This northward turn is clearer in the simulation than in the observations. The NECC water eventually turns southward and westward at the eastern end of the basin to close this equatorial gyre. West of about 180°, the NECC flows

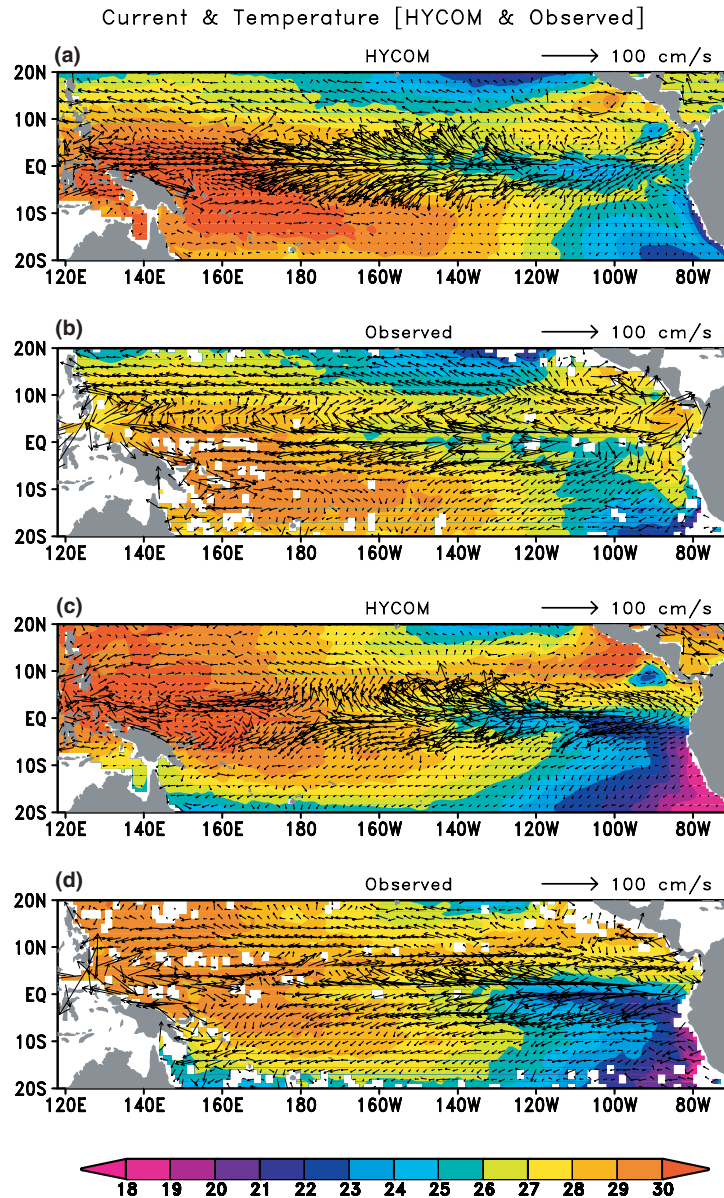Current & Temperature [HYCOM & Observed]

Fig. 1. The simulated currents and temperature at 15 m depth for (a) February and (c) August, and the satellite-tracked drifter currents and temperature for (b) February and (d) August, for the tropical Pacific Ocean. The current vectors (cm s^{-1}) are superimposed on the color temperature image (°C).

between a counterclockwise gyre to the north and clockwise gyre to the south. This double gyre structure is again more apparent in the model than in the observations.

In the simulated (Fig. 1a and c) and observed (Fig. 1b and d) temperature during February and August, the 15 m patterns are in good qualitative agreement. The western Pacific warm pool is delineated as the region warmer than 28 °C both during winter and summer, with the region

expanding northward to cover a much larger area during summer. This warm pool tends to be warmer in the simulations. In the eastern Pacific, warm water is also encountered off the coast of Central America during summer, a region considered to be part of the Western Hemisphere warm pool (Wang and Enfield, 2001, 2003). This warm pool also tends to be warmer in the simulations. In February, the model produces a cold equatorial tongue in the eastern Pacific that is colder than observed. During summer, the eastern equatorial Pacific displays an intense cold water tongue with temperature around 22 °C in both the simulation and observations, extending farther to the west in the simulation, that is mainly a result of eastern equatorial upwelling combined with westward advection of the cold water by the SEC. The southeastern region is also covered by cold water, which intensifies during boreal summer when the temperature drops to almost 18 °C. This cold water is partly a result of the upwelling occurring along the coast of Peru plus offshore advection by the SEC.

Simulated SST is further evaluated through comparison to observed Pathfinder SST. Fig. 2a and b display the SST differences (simulated minus Pathfinder) during February and August, while Fig. 2c displays the differences in annual mean SST. In general, simulated SST is about 1 °C too warm in the western Pacific warm pool region, consistent with the 15 m temperature
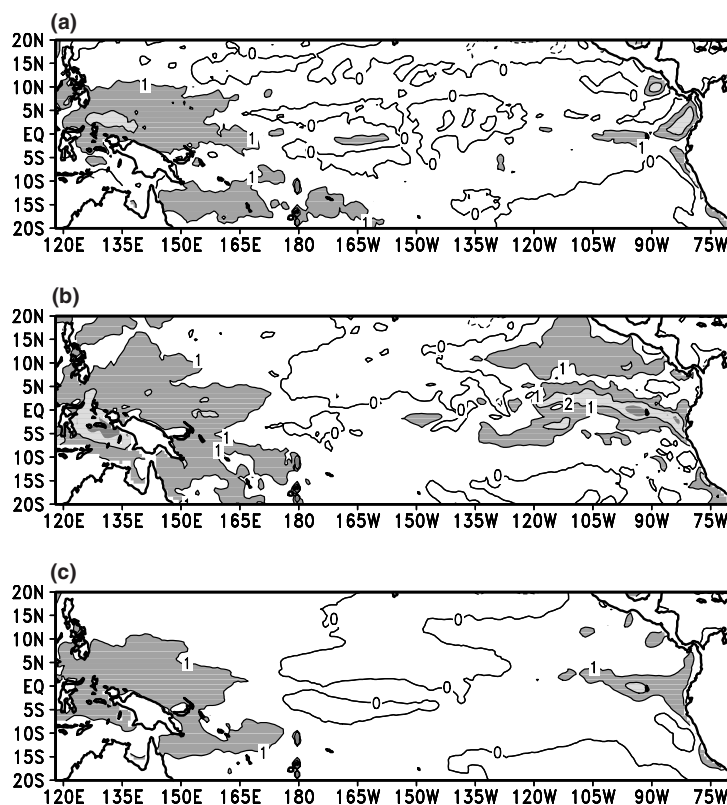

Fig. 2. The differences between simulated (with COADS forcing) and observed Pathfinder sea surface temperature (SST) (°C) for (a) February and (b) August in the tropical Pacific. The bottom panel (c) shows the differences in annual mean model and observed SST. Shading denotes temperatures greater than 1 °C.

comparison in Fig. 1. Simulated SST tends to be too warm in the eastern equatorial cold tongue region to the east of about 130°W during August, again consistent with the 15 m temperature comparison in Fig. 1. The February comparison in Fig. 2a indicates that simulated cold tongue SST is too warm only in a small band east of 105°W. This is not consistent with the 15 m temperature comparison, which indicates that simulated SST is generally too cold to the east of 140°W. This inconsistency could result in part from the different temporal averaging intervals of the two temperature climatologies. This question is further assessed in Section 5, where Levitus and Pathfinder SST are compared. In other regions, SST differences are small.

The observed temperature differences undoubtedly result in part from model biases, but forcing biases are also likely important. Recently, scientists at NOAA/AOML have processed a new forcing climatology from the Southampton Oceanography Centre where constraints have been used to correct the surface thermal forcing fields. HYCOM simulations forced with this new climatology reproduced thermal variability in the Atlantic warm pool with improved accuracy. Forcing bias also results from the use of monthly fields to drive the model and not high-frequency fields that resolve synoptic and diurnal variability.

Fig. 3 (a, b) and (c, d) show seasonal variations of surface zonal currents at 165°E and 110°W obtained from the model and drifter data respectively. Although broad agreement is evident in observed and simulated patterns, differences do exist in the location and strength of currents. At 165°E, simulated and observed westward flow associated with the NEC exists north of about 9°N, but eastward flow appears in the simulation north of about 18°N. This reversal occurs north of 20°N in the observations except during summer when the reversal occurs just south of 20°N (Fig. 3c). The model qualitatively reproduces observed semi-annual reversals of near-equatorial flow direction. The model generally underestimates current speeds south of about 10°S. An exception to this is the eastward SECC observed between 6°S and 12°S during winter, which the model reproduces realistically. Tomczak and Godfrey (1994) observed that the SECC is strongest in boreal winter with its strength gradually decreasing from west to east so that it is confined primarily to the western and central Pacific.

At 110°W, the model generally underestimates current speeds at all latitudes. The observed SEC reverses to eastward flow at the equator during spring (Fig. 3d) while the simulated flow becomes very weak but does not reverse (Fig. 3b). Although the disagreement likely results in part from model biases, forcing bias also contributes as illustrated in Section 5, where the COADS and ECMWF simulations are compared.

3.2. Subsurface circulation

Fig. 4 (a and b) depict vertical sections of model zonal currents in the upper 300 m along the equator during February and August. During February, the SEC is generally confined above 30 m in the eastern Pacific, but gradually thickens toward the west to about 100 m west of 140°E. Eastward zonal flow exists in the upper 60 m at the western end of the domain. In August, the SEC only extends westward to 160°E, and it thickens toward the east. Below the surface, the simulated EUC core is deep in the western Pacific and slopes upward to the east, with a larger slope during winter, as has been observed in earlier observational and modeling studies. In February the core velocity maximum of about 80 cm s^{-1} is located at 140°W at a depth of about 120 m. In August, two core velocity maxima exist (80 cm s^{-1} at 120°W, 120 m depth; 100 cm s^{-1}
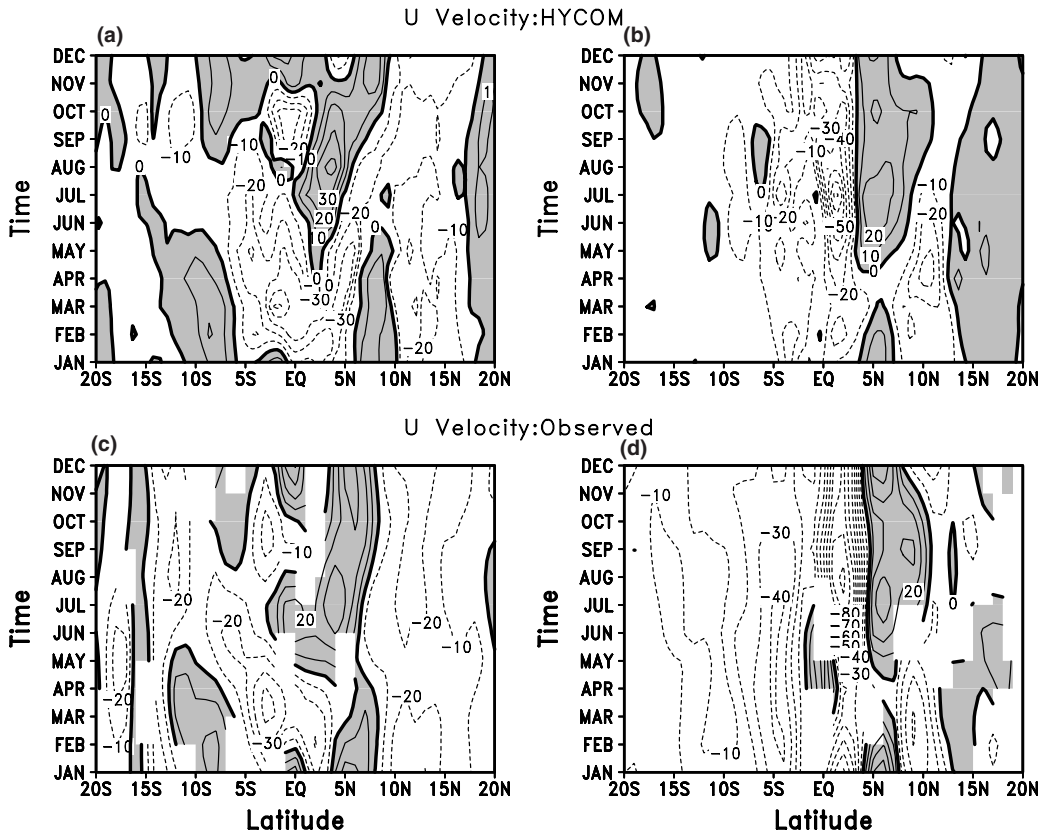
Fig. 3. Seasonal variations of the simulated zonal surface current along (a) 165°E and (b) 110°W. Seasonal variations of the observed satellite-tracked drifter zonal surface current along (c) 165°E and (d) 110°W. The unit of current is cm s⁻¹. Shading denotes eastward zonal current.

at 150°W, 120 m depth). In other model simulations, Murtugudde et al. (1996) obtained a core velocity of 160 cm s⁻¹ during March and Philander et al. (1987) obtained a core velocity of 150 cm s⁻¹ during May. Measured core velocity maxima tend to be smaller than this, but larger than the values simulated by HYCOM. Yu and McPhaden (1999) reported a core velocity maximum of 90 cm s⁻¹. This issue is discussed further in Section 3.3.

Fig. 4 (c, d) and (e, f) show the vertical sections of temperature along the equator during February and August from the simulation and the TAO array observations (Section 2) respectively. A comparison between Fig. 4 (c, d) and (e, f) indicates that the simulated temperature structure agrees rather well with the observed temperature structure along the equator. In particular, the simulation generally reproduces the depth and strength of the thermocline, along with its upward slope to the east, quite realistically. As a result, the model should accurately reproduce the resulting eastward zonal pressure gradient force along the equator that maintains the EUC (Philander, 1990). On the negative side, model isotherms tend to be deeper than observed, particularly beneath the thermocline. Also, the model underestimates the thickness of the thermocline east of about 120°W as isotherms at the base of the thermocline and below become flat instead of continuing the observed upward slope to the east of this longitude.
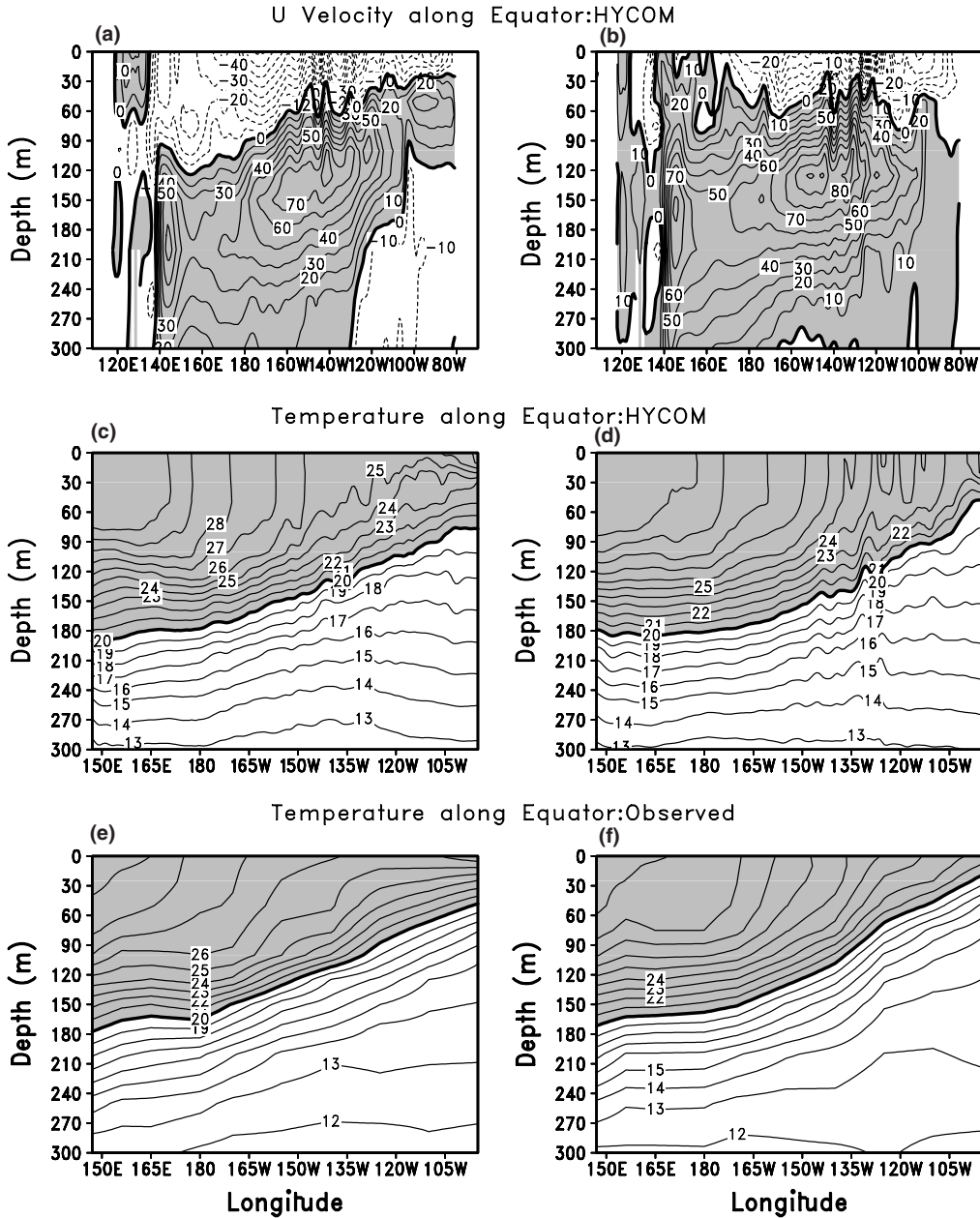
Fig. 4. Vertical section of simulated zonal current (cm s^{-1}) along the equator in the upper 300 m of the water column during (a) February and (b) August for the tropical Pacific Ocean. Vertical section of simulated temperature (°C) along the equator in the upper 300 m of the water column during (c) February and (d) August. Vertical section of observed climatological temperature (°C) along the equator in the upper 300 m of the water column during (e) February and (f) August for the tropical Pacific Ocean, obtained from the TAO array region. Shading represents eastward zonal current for velocity (upper panels) and isotherms greater than 20 °C (middle and bottom panels).
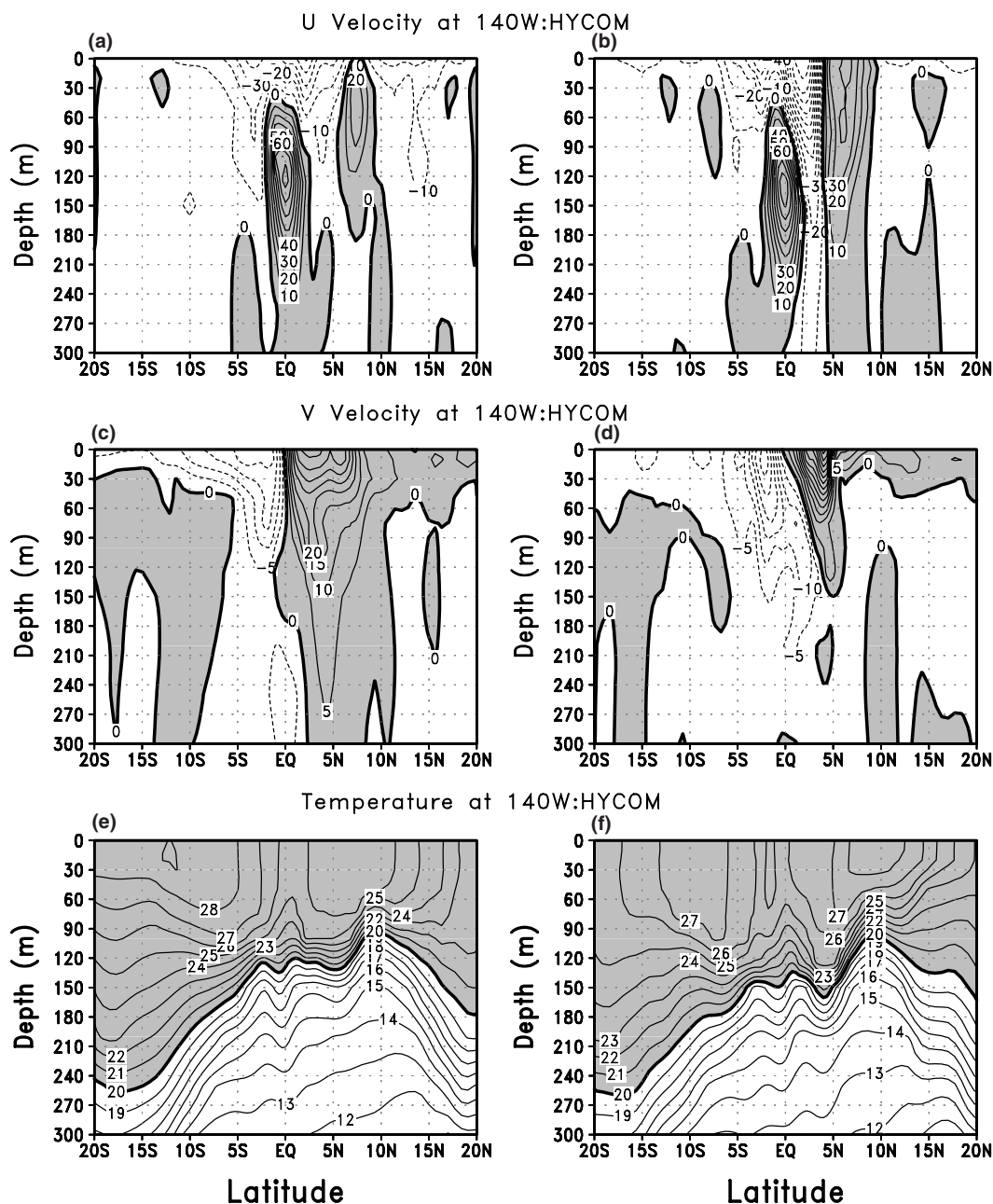
Fig. 5. Vertical section of model zonal velocity (cm s^{-1}) (a and b), meridional velocity (cm s^{-1}) (c and d) and temperature (°C) (e and f) at 140 W in the upper 300 m of the water column during February and August. Shading denotes eastward zonal flow (upper panels), northward meridional flow (middle panels) and isotherms greater than 20 °C (bottom panels).

Fig. 5 (a, b), (c, d) and (e, f) show the vertical sections of zonal velocity, meridional velocity and temperature respectively in the upper 300 m at 140°W during February and August. From Fig. 5a

and b, the SEC is confined above 40 m at the equator while it penetrates to deeper levels to the north and south. The strongest westward flow associated with the SEC is mainly concentrated between about 5°S and 5°N. In the Southern Hemisphere, weaker westward surface zonal flow exists southward to 20°S. In the Northern Hemisphere, weaker westward zonal flow extends northward to 20°N during February with the exception of eastward flow associated with the NECC near 8°N that has a maximum near 50 m and is relatively weak at the surface. During August, a strong eastward flowing NECC exists between 5 and 10°N with maximum speeds exceeding 40 cm s^{-1} above 90 m. Just below the surface SEC, the eastward flowing subsurface EUC is confined between 2°S and 2°N with maximum velocity exceeding 80 cm s^{-1} at 120 m during February and 135 m during August. During February, strong equatorial divergence between 2°S and 2°N is primarily confined above 100 m (Fig. 5c). There is no clear transition between the surface divergence and quasi-geostrophic convergence beneath it. Near surface meridional convergence is present between 5 and 15°S, and also between 6 and 14°N, which could be associated with the downwelling limbs of shallow overturning cells. During August, the axis of equatorial divergence is tilted, being on the equator at the surface, but shifting northward with depth to 3°N at 120 m. Strong meridional convergence exists from 2 to 5°S and from 4 to 7°N, suggesting that strong shallow tropical overturning cells may exist during summer.

The vertical structure of temperature at 140°W (Fig. 5e and f) shows the classical pattern inferred from earlier studies (Philander, 1990), with a shallower thermocline in the equatorial region and a trough-ridge system north of the equator associated with the NECC that is stronger during summer. South of 3°S and north of 10°N, the poleward increases in isotherm depth reflects the geostrophic balance associated with the westward-flowing SEC and NEC, respectively. The upward (downward) bowing of isotherms above (below) the EUC core within 2° of the equator reflects the equatorial quasi-geostrophic balance associated with the EUC and the SEC jet above (Philander, 1990).

3.3. Comparison with ADCP measurements

Vertical profiles of simulated equatorial zonal velocity from four selected longitudes (110°W, 140°W, 170°W, and 165°E) are compared to ADCP zonal velocity from the TAO array for four months (February, May, August, and November) to evaluate the simulated seasonal cycle of zonal equatorial flow (Fig. 6). General agreement exists between simulated and observed current profile structure at all locations, but some quantitative differences are present. At 110°W, the ADCP current values are more eastward than the simulated values year round above 125 m. As a result, there is a seasonal reversal in the SEC flow direction present in observations from mid-winter through spring that does not exist in the simulation, and the EUC core velocity is stronger in the observations throughout the year. From Fig. 4a and b, this location is at the eastern edge of the strong EUC core. Since the observed and simulated velocity profiles at the other three locations are much more similar to each other (Fig. 6), the comparatively large differences at 110°W suggest that the strong EUC core does not extend as far to the east in the simulation as it does in nature. The simulated EUC decays too rapidly at the eastern end, which is probably related to the weakening of the simulated thermocline to the east of 120°W revealed in Fig. 4.

The location 140°W is slightly west of the core of the equatorial cold-water tongue. The vertical structures of the observed and simulated zonal currents are similar at this point (Fig. 6e–h) except
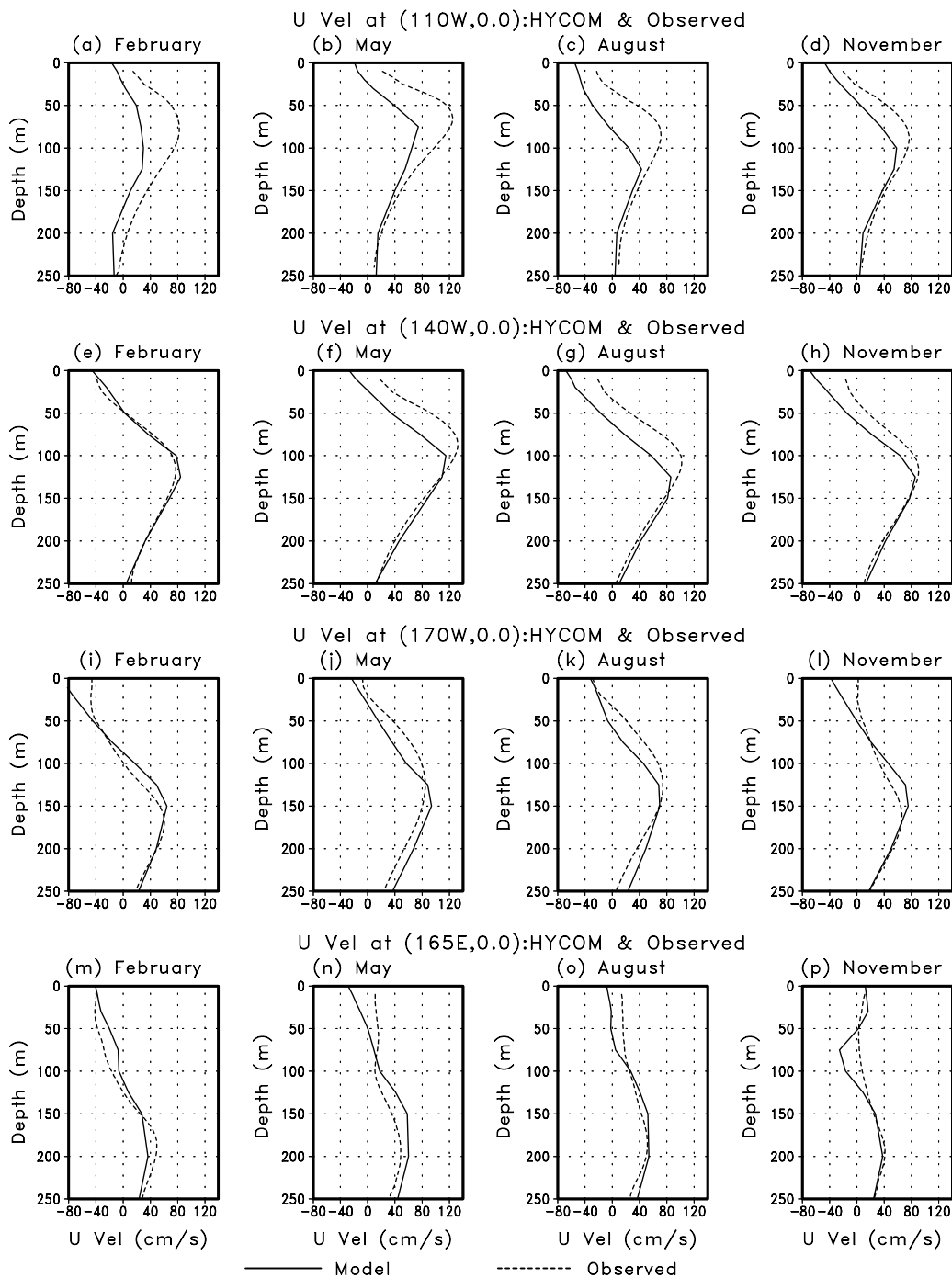
Fig. 6. The model and observed ADCP zonal velocity (cm s^{-1}) during boreal winter (February), spring (May), summer (August) and fall (November) respectively at the locations (110°W, 0) (a–d), (140°W, 0) (e–h), (170°W, 0) (i–l), and at (165°E, 0) (m–p) in the upper 250 m for the model (solid lines) and observations (dashed lines).

that the simulated flow has a westward bias above 120 m from spring through autumn. As a result, the simulated westward nearsurface SEC is stronger, and the simulated EUC core deeper and weaker, than the observed flow. The weaker EUC core velocities simulated by HYCOM here and at 110°W may also indicate that meridional grid resolution has to be increased to properly simulate the core velocity maximum. A spring surface flow reversal also occurs at this location that is not reproduced by the model. The flow differences at this location and at 110°W suggest that the surface stress forcing the model has a westward bias, or perhaps that the vertical viscosity profiles produced by the KPP vertical mixing submodel have errors that adversely affect vertical shear and hence the vertical profile of zonal current produced by the model.

The location 170°W is a transition region between the cold tongue and warm pool. As seen in Fig. 6i–l, differences between the model and observed profiles are small at this location. Core depth of the simulated EUC tends to be slightly deeper than observed during spring and summer, and slightly shallower during the remainder of the year. The location 165°E is in the warm pool region in the western equatorial Pacific where the zonal currents are not as strong. Fig. 6m–p also show reasonable similarity between simulated and observed profiles. The EUC core is much deeper here that farther to the east and the simulated EUC does not show a depth bias with respect to the observed EUC.

4. Circulation in the tropical Atlantic Ocean

The surface and subsurface circulation features in the tropical Atlantic Ocean are discussed in this section.

4.1. Surface circulation

Like the tropical Pacific Ocean, the Atlantic surface circulation is comprised of alternating bands of westward and eastward flowing zonal currents driven primarily by trade wind forcing. Fig. 7a and b show the simulated currents and temperature at 15 m depth during February and August. Fig. 7c and d show the currents and temperature during February and August from the satellite-tracked drifters. Comparisons are more difficult in the tropical Atlantic due to large spatial data gaps in the observations. Both the model and observations show the major surface zonal currents such as the westward flowing SEC and NEC and the eastward flowing NECC. The SEC is strongest within a few degrees of the equator. Most of this flow feeds the North Brazil Current (NBC) and contributes in part to the northward transport of the upper limb of the Atlantic meridional overturning circulation (Halliwell et al., 2003). The NEC, usually present north of 10°N, is a comparatively weak, predominantly zonal flow in both the simulation and observations. The model reproduces the seasonal appearance and disappearance of the NECC (Garzoli and Katz, 1983; Richardson and Walsh, 1986). Similar to the tropical Pacific Ocean, the simulated currents more than several degrees away from the equator are generally weaker than observed currents, again due in part to the lower resolution there.

In both the simulation and observations, the strongest flow is associated with the NBC. During February, the simulated and observed NBC both attain a maximum speed of about 80 cm s^{-1}. During August, both observed and simulated maximum speeds reach about 100 cm s^{-1}. During
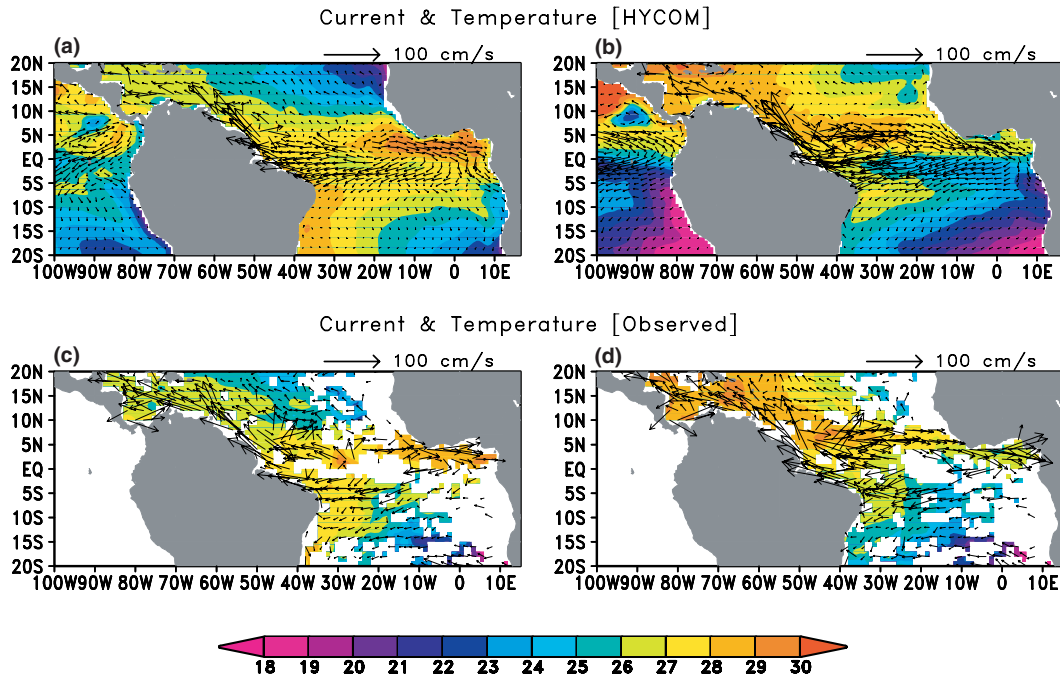
Fig. 7. The simulated currents and temperature at 15 m depth for (a) February and (b) August, and the satellite-tracked drifter currents and temperature for (c) February and (d) August, for the tropical Atlantic Ocean. The current vectors (cm s^{-1}) are superimposed on the color temperature image (°C).

February, the NECC is a weak flow at 5°N east of 25°W in both simulations and observations. During August, the NECC is strong across the entire basin, with the retroflection of the NBC supplying water to this current (Garzoli and Katz, 1983). The NECC continues its journey towards the east into the Gulf of Guinea as the Guinea Current, where it is prevented from flowing north by the African coastline and thus turns south to feed the SEC. The model faithfully reproduces the seasonal variability of this equatorial gyre structure and is also in realistic accord with other model simulations, such as that of Murtugudde et al. (1995, 1996) and Philander and Pacanowski (1986). Neither the simulation nor the observations show the SECC during February and August. Equatorial divergence is evident in both simulation and observations, and is stronger in August (Fig. 7b and d) due to stronger trade winds.

Observed and simulated temperature distributions correspond well during both February and August. During boreal summer, the northern tropical Atlantic is mainly occupied by warm water. In the Intra-Americas Sea, the temperature exceeds 28 °C, and represents the eastern part of the Western Hemisphere warm pool (Wang and Enfield, 2001, 2003). During summer, the equatorial cold tongue resulting from equatorial upwelling exists in the east-central Atlantic. It is difficult to determine the fidelity with which the simulation reproduces the cold tongue because it is poorly resolved by the observations. Comparing the few observational grid boxes in the cold tongue to the corresponding observational grid boxes suggests that model 15 m temperature is equal to or colder than the observed temperature. The temperature distribution in the South Atlantic shows some similarities with the South Pacific Ocean. In particular, marked differences from zonal

orientation also exist in the South Atlantic where the prevailing currents advect cold upwelled water offshore.

Differences between model and Pathfinder SST during February and August are presented in Fig. 8a and b, while the differences in annual mean SST are shown in Fig. 8c. The model SST is slightly higher than observed Pathfinder SST in the eastern equatorial Atlantic. In other regions in the model domain, the model SST shows a reasonable matching with the observed SST. As in the Pacific, the model is warmer by about 1–2 °C in the eastern equatorial cold tongue region during summer. This summer difference apparently contradicts the 15 m temperature comparison in Fig. 7b and d. However, that comparison was based on a very small number of common grid points and the Pathfinder SST comparison is clearly much more significant. Again, part of this difference could arise because these two observational temperature datasets (drifter and Pathfinder) have different temporal averaging intervals. This question is further assessed in Section 5 where Pathfinder and Levitus SST are compared. The annual mean SST difference also indicates warmer model SST in the eastern equatorial Atlantic (Fig. 8c).

Fig. 9a and b show the seasonal variation of simulated zonal velocity at 32°W and 10°W while Fig. 9c and d depict observed zonal currents. At 32°W during summer, both model and observations show strong eastward flow between 4°N and 6°N associated with the NECC, but with simulated flow weaker than observed. The observations show the reversal of the SEC at 32°W, between 2°S and 3°N during February to May, which, as for the Pacific is not reproduced by the model (but see results from the ECMWF forcing in Section 5). The model underestimates current speeds south of about 6°S, and this is also true at 10°W. Otherwise, the model at 10°W faithfully reproduces an eastward flowing NECC between 3°N and 5°N and westward flowing SEC between 6°S and 2°N, both attaining maximum strength during summer.
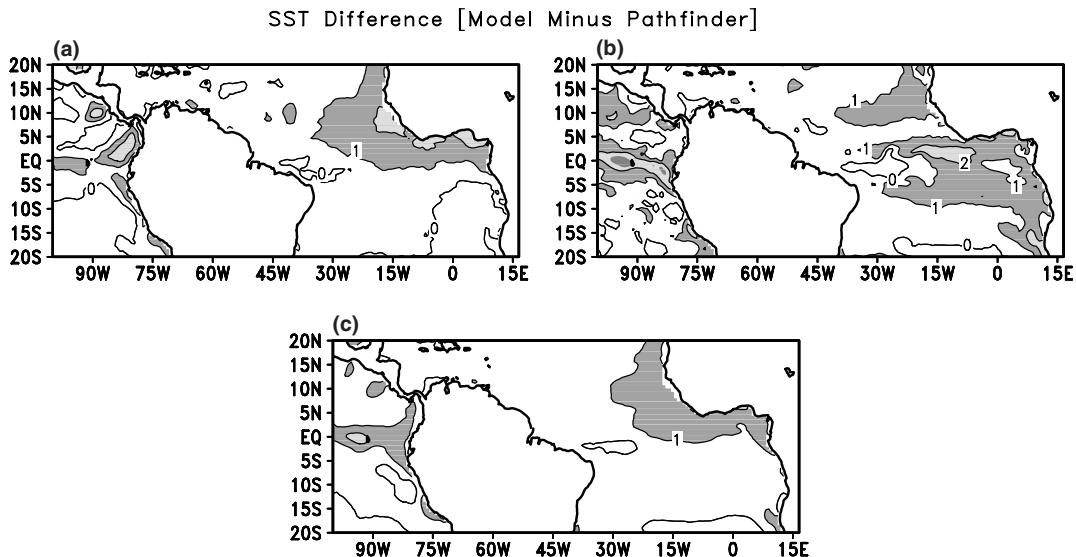

Fig. 8. The differences between simulated (with COADS forcing) and observed Pathfinder sea surface temperature (SST) (°C) for (a) February and (b) August in the tropical Atlantic. The bottom panel (c) shows the differences in annual mean model and observed SST. Shading denotes temperatures greater than 1 °C.
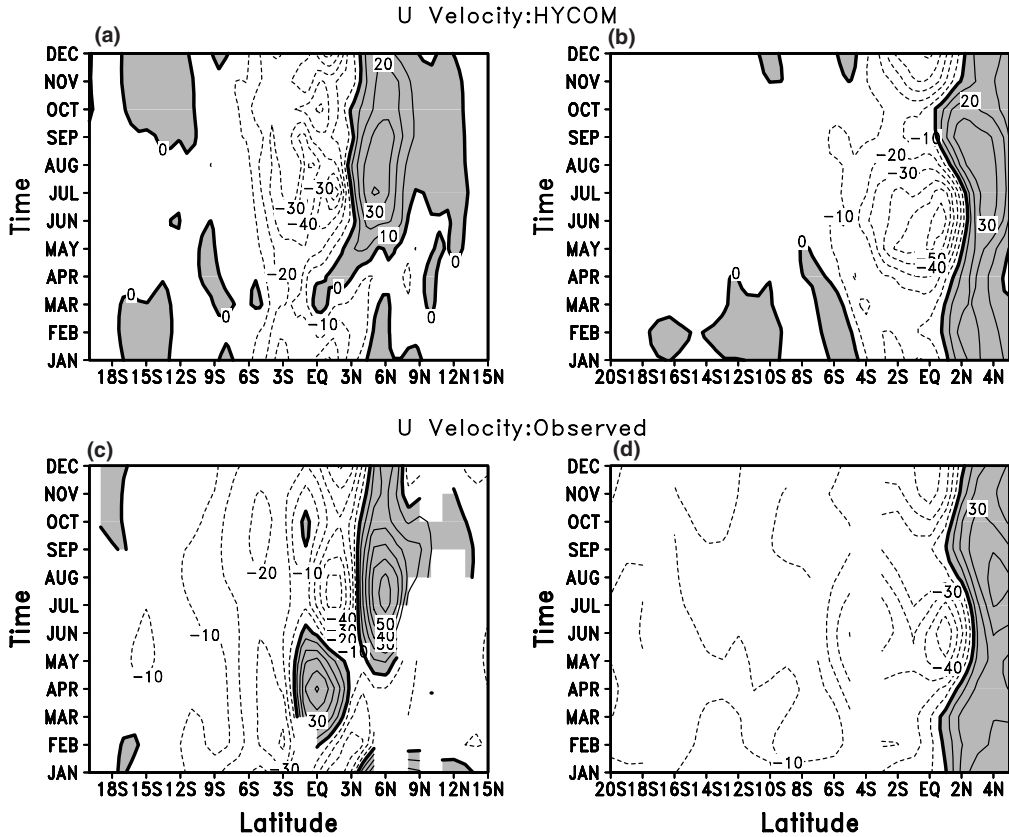
Fig. 9. Seasonal variations of the simulated zonal surface current along (a) 32°W and (b) 10°W. Seasonal variations of the observed satellite-tracked drifter zonal surface current along (c) 32°W and (d) 10°W. The unit of current is cm s^{-1}. Shading denotes eastward zonal current.

4.2. Subsurface circulation

Fig. 10a and b depict the vertical structure of zonal currents in the upper 300 m along the equator during February and August. The westward SEC at the surface and the eastward EUC below are clearly evident while the westward component of the northwestward NBC flow is evident at all depths at the western end of the basin. In February, the SEC is confined above 30 m (Fig. 10a) while in August it strengthens and thickens to 50 m (Fig. 10b). Associated with this thickening, the EUC core depth increases. Throughout the year, the EUC is deepest and strongest in the western basin while decelerating and shoaling to the east. In February, the EUC core velocity maximum exceeds 60 cm s^{-1} and is located at 35°W at a depth of 100 m. Similar to the Pacific, two core velocity maxima exist in August: one at 30°W, 115 m and the other at 38°W, 125 m. This simulated flow structure is in good agreement with previous observational studies (Philander, 1990). Model studies have produced EUCs with a wide range of maximum magnitudes, with model resolution playing a significant role, making it difficult to evaluate the present simulation. Low-resolution models tend to underestimate the core velocity, such as the 2° MICOM simulation of Chassignet
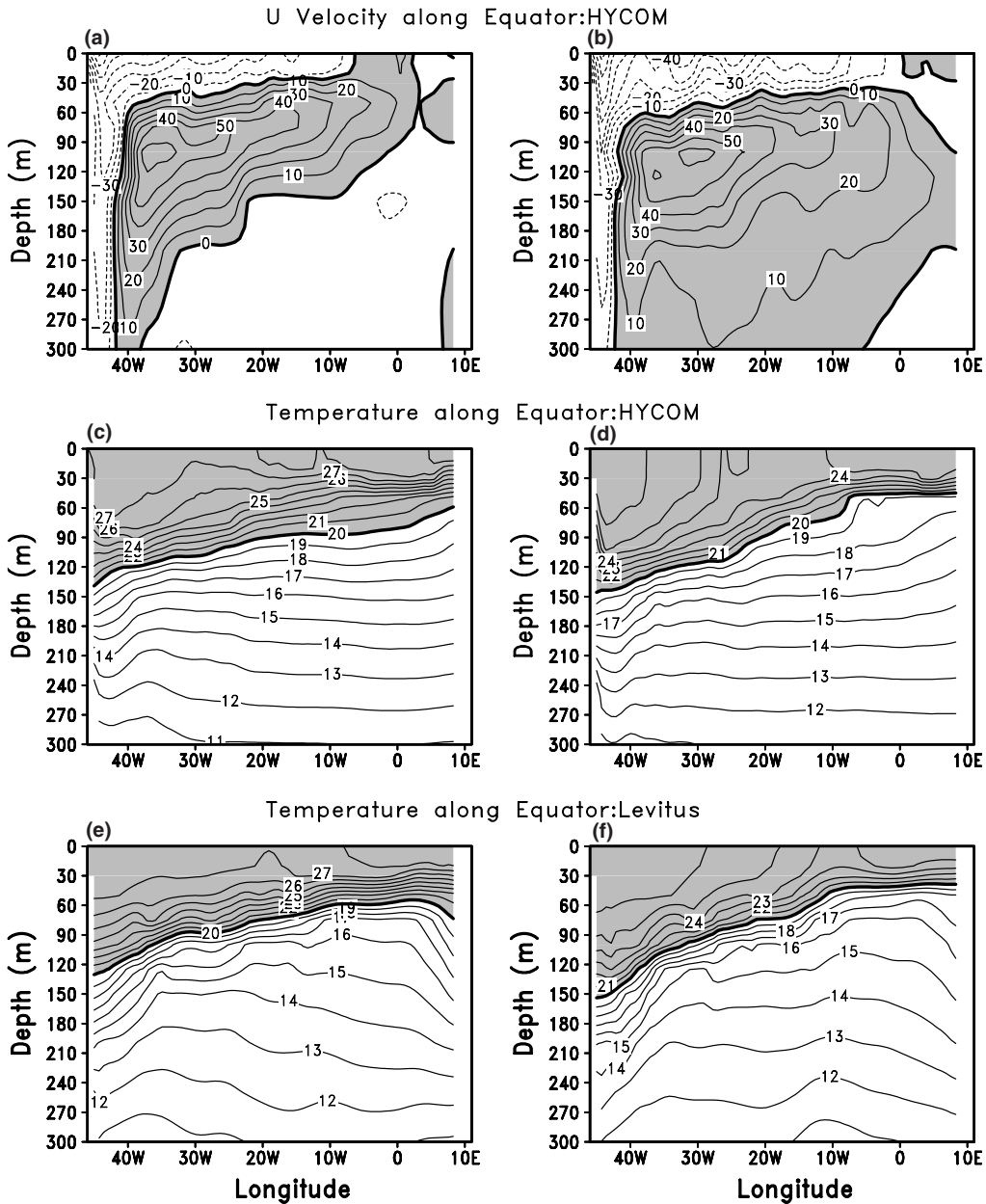
Fig. 10. Vertical section of simulated zonal current (cm s^{-1}) along the equator in the upper 300 m of the water column during (a) February and (b) August for the tropical Atlantic Ocean. Vertical section of simulated temperature (°C) along the equator in the upper 300 m of the water column during (c) February and (d) August. Vertical section of the observed climatological temperature (C) along the equator in the upper 300 m of the water column during (e) February and (f) August for the tropical Atlantic Ocean, obtained from the Levitus climatology. Shading represents eastward zonal current for velocity (upper panels) and isotherms greater than 20 °C (middle and bottom panels).

et al. (1996) (core velocity of $30 \, \text{cm s}^{-1}$) and the isopycnic model analysis of Oberhuber (1993) (core velocity of $50 \, \text{cm s}^{-1}$). In higher resolution simulations, Murtugudde et al. (1996) simulated the EUC and obtained a maximum core velocity of about $90 \, \text{cm s}^{-1}$ in March while Philander and Pacanowski (1986) obtained a core velocity of $90 \, \text{cm s}^{-1}$. Observations tend to support this larger velocity maximum (e.g., Schott et al., 1995, who measured maximum velocity exceeding $80 \, \text{cm s}^{-1}$ at 35°W). The weaker core velocity maximum simulated by HYCOM again suggests that meridional resolution must be smaller than 0.5° to properly simulate this maximum.

Fig. 10 (c, d) and (e, f) show the vertical structure of temperature along the equator during February and August obtained from the simulation and from the Levitus climatology. Both the simulated and observed thermoclines slope upward toward the east and have a larger slope in summer. Similar to the tropical Pacific Ocean, the simulated isotherms, and thus the thermocline, are deeper compared to the observed isotherms, in this case provided by the Levitus climatology instead of the TAO array. This is again most evident beneath the core of the EUC.

Fig. 11a–f show the vertical sections of zonal velocity, meridional velocity and temperature in the upper 300 m of the Atlantic Ocean at 20°W during February and August. The meridional/vertical structure of the flow (Fig. 11a and b) demonstrates that the westward flowing SEC is confined above 30 m within 5°S–3°N and exists as a thinner, weaker westward flow south of 5°S. The SEC intensifies in August between 5°S and 3°N, as does the eastward flowing NECC farther to the north. The EUC is confined between 2°S and 2°N as it is in the Pacific. During February, the EUC is confined between 30 and 130 m, with a core velocity exceeding $40 \, \text{cm s}^{-1}$ at 80 m. In August, the vertical extent of the EUC below 30 m expands substantially while the core velocity exceeds $40 \, \text{cm s}^{-1}$ at 90 m. The vertical structure of meridional velocity at 20°W (Fig. 11c and d) shows clear evidence of surface divergence near the equator during summer only, which is strongest between the surface and 90 m. There is no clear evidence of the expected quasi-geostrophic meridional convergence below. During winter, surface meridional divergence is only evident in the upper 10 m and is centered near 1°S. As for summer, there is no clear evidence of the expected quasi-geostrophic meridional convergence below on the equator.

The vertical structure of temperature at 20°W (Fig. 11e and f) generally shows the classical pattern that was observed in the Pacific (Fig. 5e and f) and inferred from earlier studies (Philander, 1990). The shallower thermocline near the equatorial is evident, but the seasonal cycle of the trough-ridge system north of the equator associated with the NECC is weak because this section is located to the east of the strongest part of the NECC. The upward (downward) bowing of isotherms above (below) the EUC core within 2° of the equator that reflects the equatorial quasi-geostrophic balance associated with the EUC and the SEC jet above (Philander, 1990) is not as strong in the Atlantic as in the Pacific.

5. Sensitivity studies

The simulations presented in Sections 3 and 4 were driven by the COADS monthly climatological surface forcing fields. In this section, we deal with model sensitivity to the forcing. For that, we performed another simulation identical to the COADS simulation except that it was driven by surface forcing fields obtained from the ECMWF ERA-15 reanalysis climatology. The ECMWF results are presented separately for the Pacific and Atlantic Oceans.
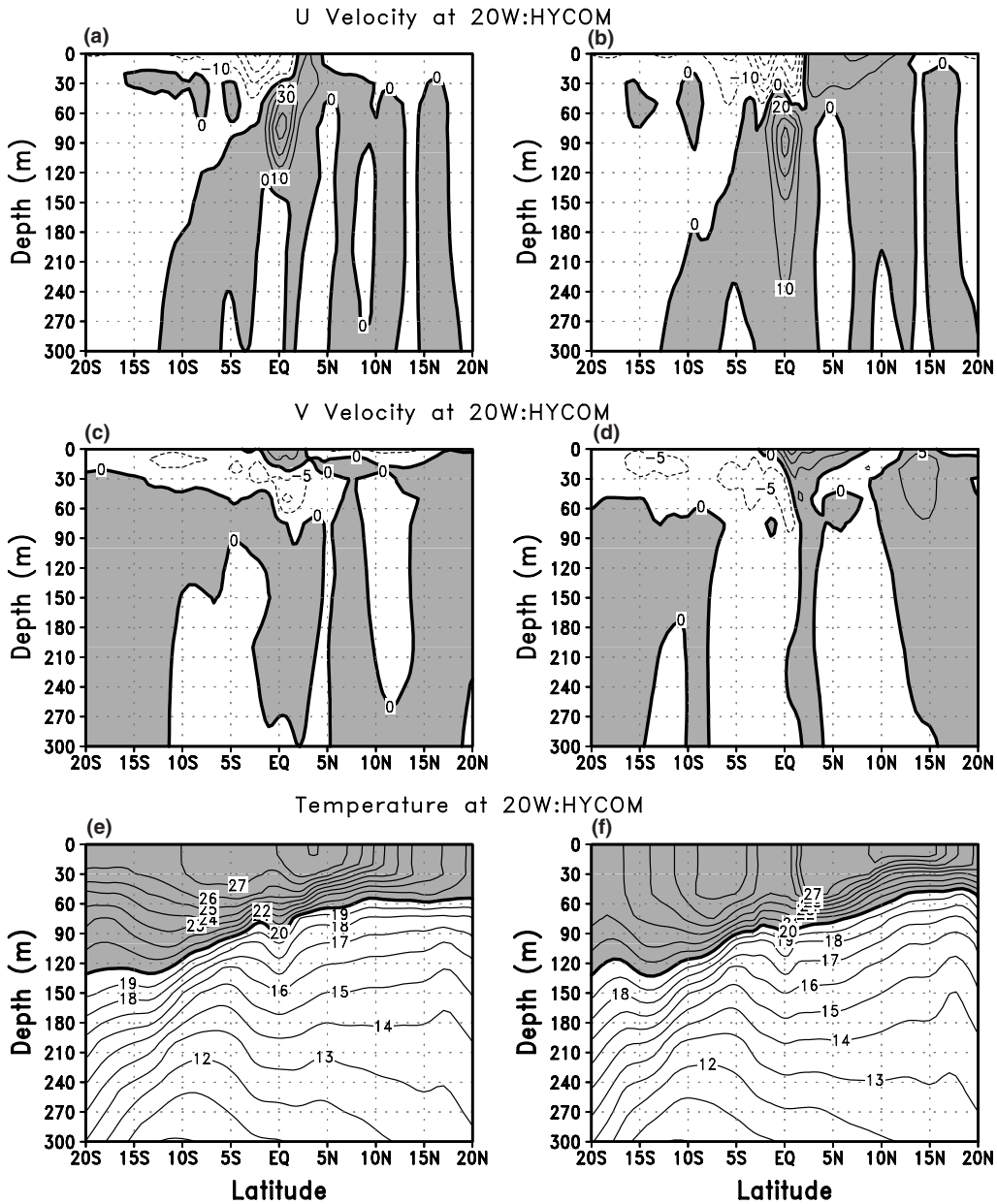
Fig. 11. Vertical section of model zonal velocity (cm s^{-1}) (a and b), meridional velocity (cm s^{-1}) (c and d) and temperature (°C) (e and f) at 20°W in the upper 300 m of the water column during February and August. Shading denotes eastward zonal flow (upper panels), northward meridional flow (middle panels) and isotherms greater than 20°C (bottom panels).

Fig. 12a and b represent the climatological annual variation of zonal velocity at the selected two points 165°E and 110°W in the tropical Pacific Oceans, and are compared to the COADS simulation and observations in Fig. 3. Although broad patterns are similar, significant quantitative
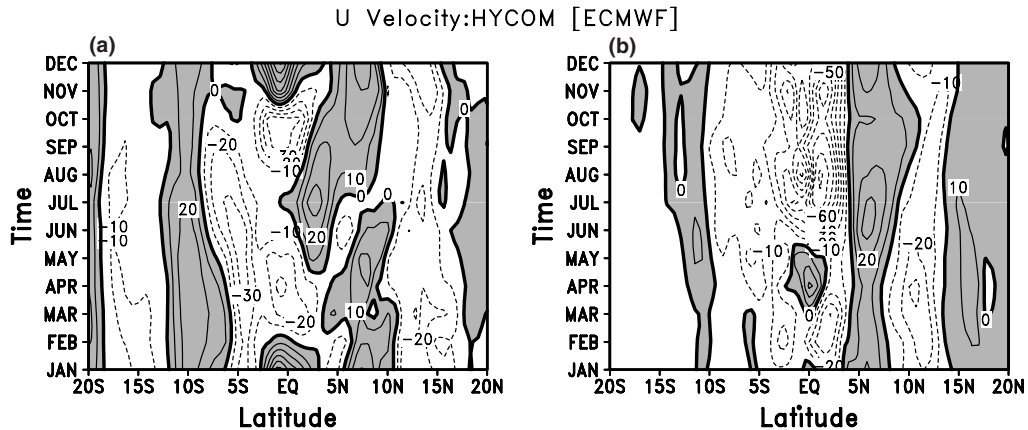
U Velocity:HYCOM [ECMWF]

Fig. 12. Seasonal variations of the simulated zonal surface current along (a) 165°E and (b) 110°W based on the simulation with ECMWF forcing. The unit of current is cm s^{-1}, and shading denotes eastward zonal flow. These figures can be compared with those from the COADS simulation (Fig. 3a and b) and those from the observed drifter data (Fig. 3c and d).

differences exist between the two simulations that are similar in magnitude to differences between each simulation and the observations. For example, at 165°E, the SECC is strongest in winter, consistent with the COADS simulation, but is present between 5°S and 12°S throughout the year in the ECMWF run (Fig. 12a) instead of being confined to winter and early spring (Fig. 3). At 110°W, the simulated SEC shows a reversal during spring that is consistent with observations (Fig. 3d) and that is not present in the COADS simulation (Fig. 3b). These results demonstrate that model–data differences result as much from forcing errors and biases as from model limitations.

Fig. 13a and b display the wind stresses during August from the COADS and ECMWF reanalysis climatology. Almost everywhere in the domain, the COADS winds are stronger than the ECMWF winds. In Fig. 13c, simulated August SST along the equator for the COADS and ECMWF runs are compared with the observed Pathfinder and Levitus SST. Differences between the simulations and observations primarily exist in the western warm pool region west of the date line and in the cold tongue region east of 120°W as noted earlier. SST from the COADS simulation is slightly larger between 140°E and 160°E, and smaller between 110°W and 92°W, than SST from the ECMWF simulation. In the western warm pool region, Pathfinder SST is equal to or warmer than Levitus SST. Differences between simulations and observations are larger than the differences between the two simulations and between the two observational datasets, indicating model limitations are primarily responsible for the warmer simulated SSTs in the warm pool. In the cold tongue region east of 120°W, simulated SST again tends to be too warm. In this region, however, differences between the two simulations and between the two observational datasets are larger than in the warm pool region, so factors other than model limitations play a more important role in the cold tongue. Forcing errors likely make a significant contribution due to the SST differences between the COADS and ECMWF cases. Also, the temporal averaging intervals of the model forcing climatologies and the SST observational climatologies are different. Since these different temporal intervals do not include the same ENSO cycles, cold-tongue SST
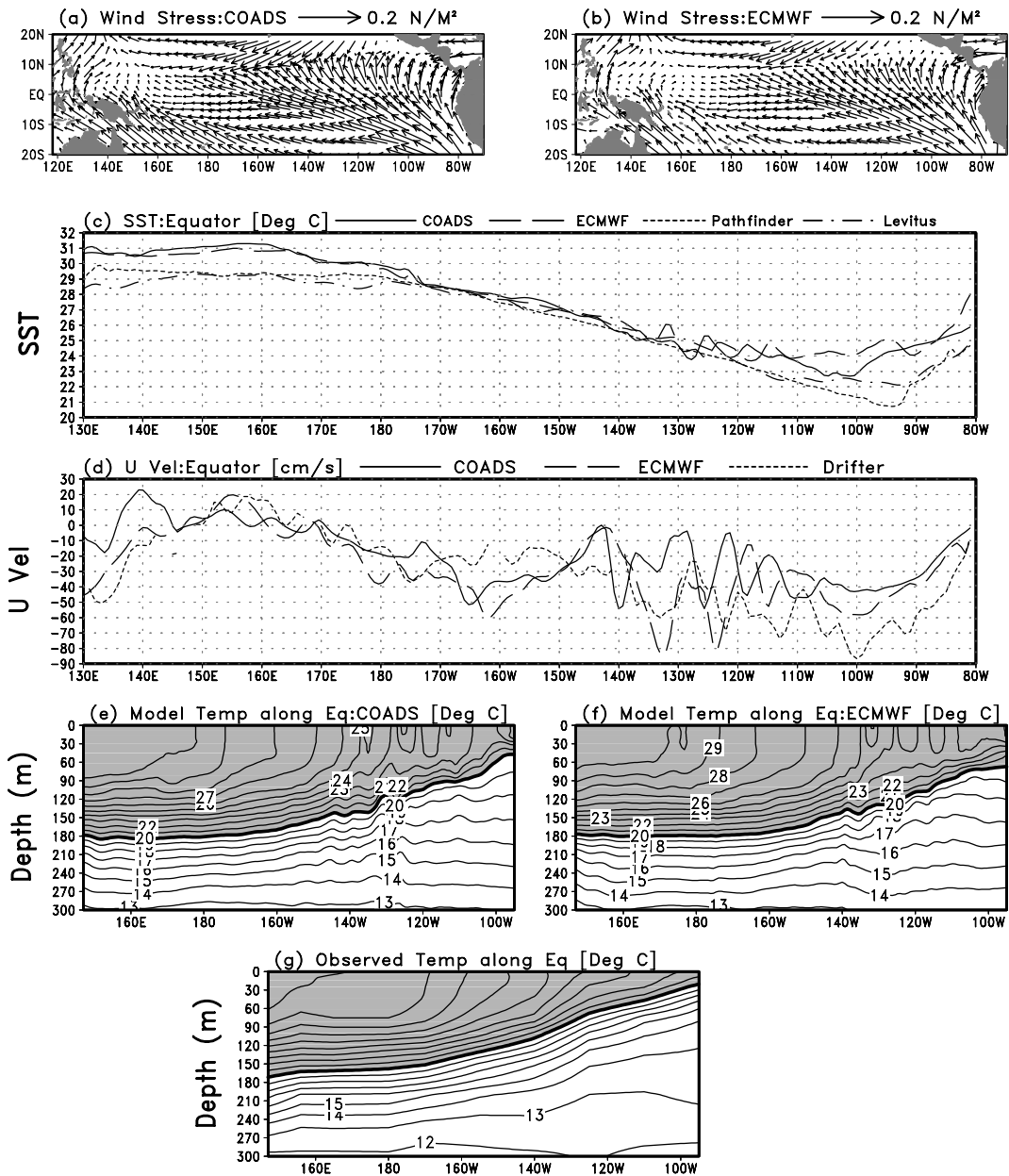
Fig. 13. The climatological monthly mean wind stress during August from (a) COADS and (b) ECMWF reanalysis climatology in the tropical Pacific Ocean. The second panel (c) shows comparing model simulated SST from the COADS and ECMWF simulations with the observed Pathfinder and Levitus SST along the equator during August. The third panel (d) shows comparing model simulated zonal velocity from the COADS and ECMWF simulations with the drifter data along the equator during August. Vertical section of simulated temperature along the equator in the upper 300 m of the water column during August from the (e) COADS and (f) ECMWF simulations and its comparison with the observed (g) TAO temperature. Shading in figures e–g denotes isotherms greater than 20 °C.

simulated by the model and mean SST from the observational datasets will differ to some extent even if a perfect model is used.

Fig. 13d shows the simulated zonal velocity at 15 m depth along the equator during August from the COADS and ECMWF simulations, and also from the drifter data, revealing the westward-flowing SEC east of 175°E. In general, differences between the simulations are as large as differences between each simulation and the observations. Simulated westward zonal velocity associated with the SEC is generally smaller than observed zonal velocity east of 120°W. Fig. 13e and f show vertical sections of simulated temperature along the equator during August from the COADS and ECMWF forcing while Fig. 13g shows the observed TAO temperature along the equator during August. In general, the isotherms from the ECMWF simulation are slightly deeper compared to the COADS simulation, and thus slightly less realistic compared to observations. The COADS run produces a thermocline with a larger upward slope toward the east that is closer to observations (Fig. 13g).

For the Atlantic, Fig. 14a and b show the climatological annual variation of zonal velocity simulated with ECMWF forcing at 32°W and 10°W, which are compared to the COADS run and observations in Fig. 9. Although broad patterns are similar as they were in the Pacific, significant quantitative differences exist between the two simulations that are again similar in magnitude to differences between each simulation and the observations. For example, at 32°W, the spring reversal of the SEC at the equator is more clearly evident in the ECMWF simulation (Fig. 14a) as compared to the COADS run (Fig. 9a), and this reversal is more consistent with the observations (Fig. 9c). The ECMWF forcing generated a stronger SEC during summer at 10°W (Fig. 14b) compared to the COADS simulation (Fig. 9b), the latter being closer to observations (Fig. 9d).

Fig. 15a and b display wind stresses during August from the COADS and ECMWF climatologies. As in the Pacific Ocean, the COADS winds are stronger compared to the ECMWF winds. The simulated SST along the equator during August for the COADS and ECMWF runs, along
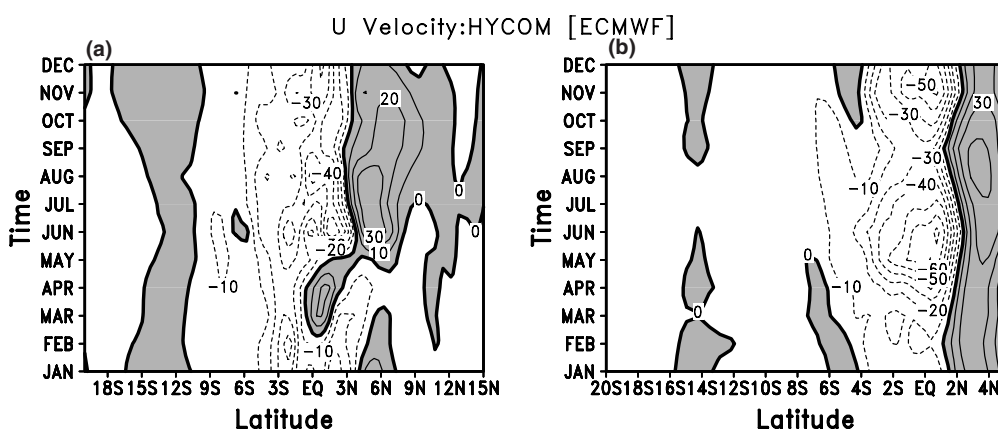

Fig. 14. Seasonal variations of the simulated zonal surface current along (a) 32°W and (b) 10°W based on the simulation with ECMWF forcing. The unit of current is cm s^{-1}, and shading denotes eastward zonal flow. These figures can be compared with those from the COADS simulation (Fig. 9a and b) and those from the observed drifter data (Fig. 9c and d).
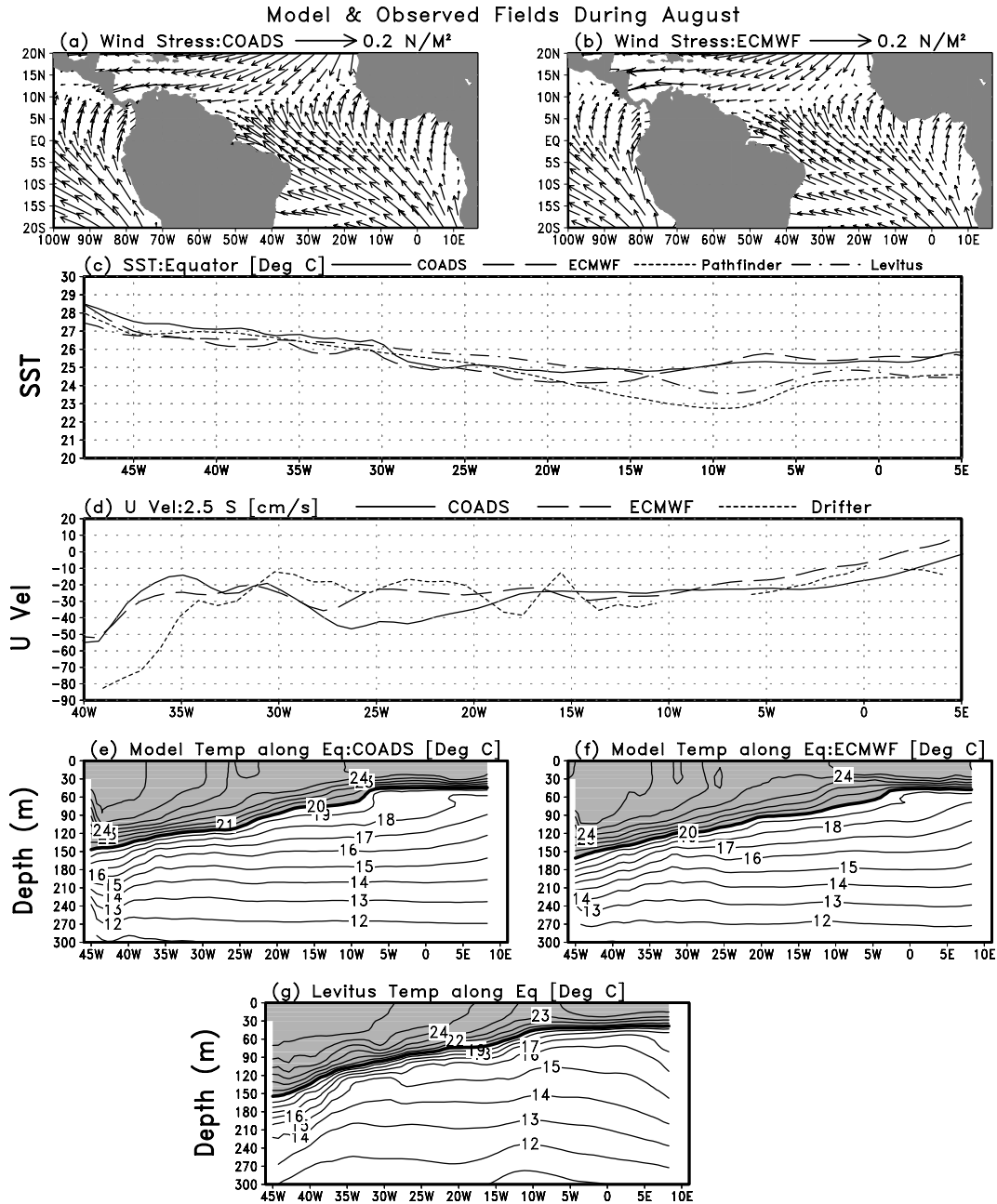
Model & Observed Fields During August

Fig. 15. The climatological monthly mean wind stress during August from (a) COADS and (b) ECMWF reanalysis climatology in the tropical Atlantic Ocean. The second panel (c) shows comparing model simulated SST from the COADS and ECMWF simulations with the observed Pathfinder and Levitus SST along the equator during August. The third panel (d) shows comparing model simulated zonal velocity from the COADS and ECMWF simulations with the drifter data along 2.5°S during August. Vertical section of simulated temperature along the equator in the upper 300 m of the water column during August from the (e) COADS and (f) ECMWF simulation and its comparison with the (g) Levitus climatological temperature. Shading in figures (e–g) denotes isotherms greater than 20 °C.

with the observed Pathfinder and Levitus SST, are shown in Fig. 15c. Both the COADS and ECMWF simulations reveal zonal oscillations of SST along the equator. These oscillations may result from the existence of tropical instability wave variability. West of 30°W, SST from the COADS run is slightly warmer than observations while SST from the ECMWF run is slightly colder. East of 13°W, simulated SST is warmer than observed. East of 30°W, Levitus SST is warmer than Pathfinder, with the difference exceeding 1°C near 15°W. As for the Pacific Ocean, both forcing biases and differences in the temporal averaging intervals of the model forcing and SST climatology contribute to the SST differences in the Atlantic cold tongue region. However, model limitations also contribute to SST errors in the cold tongue, probably resulting in part from the tendency of HYCOM to produce a thermocline that is too deep in the eastern equatorial region, as was also the case in the Pacific.

The zonal flow along 2.5°S during August at 15 m depth simulated with the COADS and ECMWF forcing are compared with the drifter data at 15 m depth (Fig. 15d). This latitude is chosen because of the poor observational sampling along the equator (Fig. 7). East of 15°W, the SEC magnitude in both simulations compare favorably to each other and to observations. However, these agreements are not as good west of 15°W. West of 35°W, the magnitude of SEC is higher than the simulations. Fig. 15d also reveals zonal oscillations in the zonal flow field along 2.5°S in both simulations. This can also be due to the effect of tropical instability wave variability. The vertical structure of temperature along the equator during August from the COADS and ECMWF simulations (Fig. 15e and f) are compared with the Levitus temperature (Fig. 15g). As for the Pacific, the COADS simulation produces a slightly shallower thermocline than the ECMWF simulation, with the shallower depth being in closer agreement with climatology.

This two-ocean comparison between two simulations driven by different climatological forcing sets demonstrates that forcing accuracy can be as important as model limitations in producing errors and biases in simulated fields, making it difficult to judge standalone model performance. Although some aspects of the ECMWF simulation were superior, such as the spring SEC reversal at the equator in both the Atlantic and Pacific Oceans, careful evaluation of the three-dimensional temperature and flow structures convinced us that the COADS simulation was closer to observations in more respects than the ECMWF simulation, particularly in regards to SST and subsurface thermal fields.

6. Summary

The purpose of this study was to evaluate capabilities and limitations of a new ocean model (HYCOM) configured on a non-uniform horizontal grid spanning 30°S–65.5°N and 102°E–15°E to simulate the climatological annual cycle of the tropical Pacific and Atlantic Oceans. Monthly climatological surface fields obtained from the COADS data are used to drive the primary simulation. Sensitivity to forcing is considered by comparing the primary COADS simulation to another driven by the ECMWF ERA-15 monthly reanalysis climatology that is otherwise identical to the primary simulation. The upper-ocean currents, temperature and many features of the tropical ocean thermocline are in general realistically modeled. One goal was to evaluate the use of latitude dependent meridional resolution that provides enhanced resolution near the equator (0.72° zonal by 0.36° meridional). The importance of enhanced resolution is evident because

HYCOM substantially underestimated zonal current magnitudes away from the equator where both zonal and meridional resolution was low.

In the Pacific Ocean, the presence and seasonality of the major surface zonal currents such as the SEC, NEC, NECC and SECC are in good correspondence with the observations. Both model and drifter velocities show the SEC accelerating along the equator from east to west, with meridional divergence associated with equatorial upwelling present all year but strongest in summer. Analysis of the annual cycle of zonal equatorial currents discloses a spring reversal of the SEC at 110°W in the observations. The COADS simulation does not reproduce this reversal, but the ECMWF does (albeit too weak). The occurrence and seasonality of the EUC has been very realistically modeled except for the tendency of the core velocity to be somewhat too weak, and also the fact that the simulated EUC terminates a few degrees farther to the west than observed. Insufficient meridional resolution could contribute to both of these shortcomings. The model also reproduces zonal and meridional slopes, ridges, and troughs in the thermocline, including their strong seasonal variations. Both the modeled and observed thermal structure shows a fairly strong thermocline along the equator, with a downward slope towards the west. The depth of the equatorial thermocline tends to be slightly deeper than observed. The model generally does a good job in simulating the seasonal evolution of off-equatorial zonal currents associated with the thermocline ridges and troughs except for the tendency to underestimate magnitudes. The warm and cold water regions and their seasonality in the tropical Pacific has been realistically simulated by the model and is in good agreement with the drifter data. A comparison of simulated SST with the observed SST climatologies reveals that simulated SST is warmer than the observations in the eastern equatorial cold tongue and in the warm pool waters of the western Pacific and also the eastern Pacific (the western limb of the Western Hemisphere warm pool). The temperature difference in the warm pool regions is similar no matter which observed temperature climatology is used for the comparison, indicating that model biases are the primary problem. The magnitude of the temperature difference in the cold tongue varies depending on the temperature climatology used for the comparison. This indicates that the different temporal averaging intervals used for these climatologies, which can differ from the temporal averaging interval of the atmospheric forcing climatologies used to drive the model, contribute in part to the cold tongue temperature differences (i.e., they are averaged over different sets of ENSO events).

In the tropical Atlantic Ocean, the model captured all the major currents such as the SEC, NEC, NECC and NBC. The highest current speeds are observed in the NBC in both the simulation and drifter velocity climatology. During winter, NECC is weak and mainly concentrated in the eastern equatorial Atlantic Ocean. During summer, this current is intensified and is supplied by the retroflection of the NBC around 5°N. The SEC indicates divergence at the equator, which is quite strong during summer and enhances the equatorial upwelling at this time. At 32°W, the drifter data shows the spring reversal of the SEC near the equator. As for the Pacific, this reversal was present in the HYCOM simulation driven by ECMWF (albeit too weak), but not in the simulation driven by COADS. As for the Pacific, the simulated EUC tends to be a little too deep and too slow, with resolution again probably contributing to the underestimate of core velocity magnitude. The simulated surface warm pool and cold tongue areas and their seasonal changes in the tropical Atlantic Ocean are generally in good agreement with the drifter temperature climatology. The temperature distribution in the Atlantic Ocean shows some similarities with the Pacific Ocean, particularly south of the equator where surface temperatures are much the same in both

the oceans. As for the Pacific, model SST is slightly warmer in the eastern equatorial cold tongue. The temporal averaging interval of the climatology used for the comparison is again a factor in the magnitude of the observed–simulated temperature difference. The tendency for isotherms to be too deep at the equator is larger in the Atlantic than in the Pacific. This problem could be related to too much vertical mixing, or could result from water with the wrong temperature converging toward the equator at depth. If the latter is true, then model biases off the equator contribute to the observed equatorial biases.

Differences in the circulation pattern and temperature distribution in the tropical Pacific and Atlantic Oceans arising from the use of ECMWF forcing were documented. In addition to the spring SEC reversal differences mentioned above, the simulation with the ECMWF forcing showed the presence of the SECC in the western Pacific throughout the year, with its peak occurring during winter. The ECMWF simulation generated higher SST in the eastern equatorial Pacific compared to the COADS simulation. A comparison of equatorial zonal flow in the Pacific Ocean from the two simulations showed marked differences, especially in the east-central and western equatorial regions. The isotherms are deeper in the ECMWF forcing simulation. In both the tropical Pacific and Atlantic Oceans, the COADS surface wind stress is stronger than the ECMWF wind stress. In contrast, SST and subsurface temperatures in the COADS case compared more favorably to observations, leading us to choose the COADS case as the primary experiment. Overall, model performance is encouraging, and we anticipate that future experiments conducted with different vertical mixing choices, different vertical coordinate choices, different horizontal advection schemes, and modifications in other model subgrid-scale parameterizations, in conjunction with improved high-frequency forcing, will produce substantially improved simulations.

Acknowledgments

References

Bleck, R., 2002. An oceanic general circulation model framed in hybrid isopycnic-Cartesian coordinates. Ocean Modell. 4, 55–88.
Busalacchi, A.J., O'Brien, J.J., 1980. The seasonal variability in a model of the tropical Pacific. J. Phys. Oceanogr. 10, 1929–1951.
Casey, K.S., Cornillon, P., 1999. A comparison of satellite and in situ based sea surface temperature climatologies. J. Climate 12, 1848–1863.
Chassignet, E.P., Smith, L.T., Halliwell, G.R., Bleck, R., 2003. North Atlantic Simulations with the Hybrid Coordinate Ocean Model (HYCOM): impact of the vertical coordinate choice, reference density, and thermobaricity. J. Phys. Oceanogr. 33, 2504–2526.

Chassignet, E.P., Smith, L.T., Bleck, R., Bryan, F.O., 1996. A model comparison: numerical simulations of the north and equatorial Atlantic oceanic circulation in depth and isopycnic coordinates. J. Phys. Oceanogr. 26, 1849–1867.

Chen, D., Rothstein, L., Busalacchi, A., 1994. A hybrid vertical mixing scheme and its application to tropical ocean models. J. Phys. Oceanogr. 24, 2156–2179.

Cox, M.D., 1984 A primitive equation three-dimensional model of the ocean. NOAA Tech. Rep. 1, GFDL/NOAA, Princeton University, NJ, 144pp.

Evans, R., Podesta, G., 1996. AVHRR pathfinder SST approach and results. EOS 77 (46).

Garzoli, S.L., Katz, E.J., 1983. The forced annual reversal of the Atlantic North Equatorial Countercurrent. J. Phys. Oceanogr. 13, 2082–2090.

Gibson, J.K., Kallberg, P., Uppala, S., Hernandez, A., Nomura, A., Serrano, E., 1999: ECMWF Re-analysis Project Report Series: 1. ERA-15 Description (version 2—January 1999). ECMWF. Reading, Berkshire, UK, 77pp.

Halliwell Jr., G.R., 2004. Evaluation of vertical coordinate and vertical mixing algorithms in the Hybrid-Coordinate Ocean Model (HYCOM). Ocean Modell. 7, 285–322.

Halliwell Jr., G.R., Weisberg, R.H., Mayer, D.A., 2003. A synthetic float analysis of upper-limb meridional overturning circulation interior ocean pathways in the tropical/subtropical Atlantic Ocean. In: Goni, G., Malanotte-Rizzoli, P. (Eds.), Interhemispheric Water Exchange in the Atlantic. Elsevier Publishing Company, pp. 93–136.

Langlois, G., Brydon, D., Bleck, R., Dean, S., 1997. Miami Isopycnic Coordinate Ocean Model (MICOM) User's Manual.

Large, W.G., Mc Williams, J.C., Doney, S.C., 1994. Oceanic vertical mixing: review and a model with a nonlocal boundary layer parameterization. Rev. Geophys. 32, 363–403.

Levitus, S., Boyer, T., 1994. World Ocean Atlas 1994, Volume 4: Temperature. NOAA Atlas NESDIS 4. US Dept. of Commerce, Washington, DC.

Levitus, S., Burgett, R., Boyer, T., 1994. World Ocean Atlas 1994, Volume 3: Salinity. NOAA Atlas NESDIS 3. US Dept. of Commerce, Washington, DC.

Lu, P., McCreary, J.P., Klinger, B.A., 1998. Meridional circulation cells and the source waters of the Pacific equatorial undercurrent. J. Phys. Oceanogr. 28, 62–84.

Lumpkin, R., 2003. Decomposition of surface drifter observations in the Atlantic Ocean. Geophys. Res. Lett. 30, 14, doi:10.1029/2003GL017519.

McPhaden, M.J., et al., 1998. The Tropical Ocean Global Atmosphere (TOGA) observing system: a decade of progress. J. Geophys. Res. 103, 14169–14240.

Mellor, G.L., Yamada, T., 1982. Development of a turbulence closure model for geophysical fluid problems. Rev. Geophys. Space Phys. 20, 851–875.

Murtugudde, R., Cane, M., Prasad, V., 1995. A reduced gravity, primitive equation, isopycnal ocean GCM: formulation and simulations. Mon. Weather Rev. 123, 2864–2887.

Murtugudde, R., Seager, R., Busalacchi, A., 1996. Simulation of the tropical oceans with an ocean GCM coupled to an Atmospheric Mixed Layer Model. J. Climate 9, 1795–1815.

Niiler, P., 2001. The world ocean surface circulation. In: Siedler, G., Church, J., Gould, J. (Eds.), Ocean Circulation and Climate, International Geophysics Series 77. Academic Press.

Niiler, P.P., Kraus, E.B., 1977. One-dimensional models of the upper ocean. In: Kraus, E.B. (Ed.), Modelling and Prediction of the Upper Layers of the Ocean. Pergamon, New York, pp. 143–172.

Oberhuber, J., 1993. Simulation of the Atlantic circulation with a coupled sea ice-mixed layer-isopycnal general circulation model, part II: model experiment. J. Phys. Oceanogr. 17, 1986–2002.

Philander, S.G., 1990. El Nino, La Nina, and the Southern Oscillation. Academic Press Inc., San Diego, California, 293pp.

Philander, S.G., Pacanowski, R., 1986. A model of the seasonal cycle in the tropical Atlantic Ocean. J. Geophys. Res. 91, 14192–14206.

Philander, S.G., Hurlin, W., Seigel, A., 1987. Simulation of the seasonal cycle of the tropical Pacific Ocean. J. Phys. Oceanogr. 17, 1986–2002.

Price, J.F., Weller, R.A., Pinkel, R., 1986. Diurnal cycling: observations and models of the upper ocean response to diurnal heating, cooling and wind mixing. J. Geophys. Res. 91, 8411–8427.

Richardson, P.L., Walsh, D., 1986. Mapping climatological seasonal variations of the surface currents in the tropical Atlantic using ship drifts. J. Geophys. Res. 91, 10537–10550.

Schott, F.A., Stramma, L., Fischer, J., 1995. The warm water inflow into the western tropical Atlantic boundary regime, spring 1994. J. Geophys. Res. 100, 24745–24760.

Sun, S., Bleck, R., Rooth, C., Dukowicz, J., Chassignet, E., Killworth, P., 1999. Inclusion of thermobaricity in isopycnic-coordinate ocean models. J. Phys. Oceanogr. 29, 2719–2729.

Tomczak, M., Godfrey, J.S., 1994. Regional Oceanography: An Introduction. Pergamon, 422pp.

Turner, J.S., Kraus, E.B., 1967. A one-dimensional model of the seasonal thermocline II: the general theory and its consequences. Tellus 18, 98–105.

Wang, C., Enfield, D.B., 2001. The tropical Western Hemisphere warm pool. Geophys. Res. Lett. 28, 1635–1638.

Wang, C., Enfield, D.B., 2003. A further study of the tropical Western Hemisphere warm pool. J. Climate 16, 1476–1493.

Woodruff, S.D., Sultz, R.J., Jenne, R.L., Steurer, P.M., 1987. A comprehensive ocean-atmosphere data set. Bull. Amer. Meteor. Soc. 68, 1239–1250.

Yu, X., McPhaden, M.J., 1999. Seasonal variability in the equatorial Pacific. J. Phys. Oceanogr. 29, 925–947.